Electronic Supplementary Material (ESI) for Journal of Materials Chemistry A.

Supporting Information

Protic ethers as highly efficient hydrogen-bond regulators for aqueous eutectic electrolytes

Xuejun Lu [a], [+] Zhenhua Liu [b], [+] Li Tao [a], Hao Sun [b]*, Yulong Liu [b], Jian Liu [a]*

Experimental

Preparation of aqueous Li-based eutectic (ALE) electrolytes

All chemicals and reagents were analytical grade and used without further purification. The samples preparation process can be referred to previous work, [1] where all ALE-based electrolytes were synthesized in molality (mol kg^{-1}) of the resulting solutions.

Characterizations

NMR measurements were carried out on an AVANCE III 400MHz equipment with BBO probe, samples were placed in NMR tubes and analyzed using a separated capillary tube with deuterated methanol (CD_3OD) as the external reference. Differential scanning calorimetry (DSC) analyses were performed in a TA instrument DSC-Q1000 under a N_2 atmosphere. FTIR spectra was performed using EO-SXB IR spectrometer. Raman spectra were recorded using a SENTERRA II model with an excitation wavelength of 532 nm. Contact angle tests were obtained from a goniometer with OCA 15 model.

Electrochemical Measurements

The ionic conductivity of ALE-based electrolytes was tested at room temperature and –20 °C by two symmetric blocking stainless steel (SS) electrodes and calculated according to equation [1]:

$$\kappa = L/(R \cdot A) \quad [1]$$

where L and A are the thickness and effective contacting area between SS electrode and electrolyte, respectively, and R is the resistance obtained by electrochemical impedance spectroscopy (EIS) test.

All electrochemical measurements including cyclic voltammetry (CV), galvanostatic charge-discharge (GCD), and EIS were performed using a VSP-3e Potentiostat. Coin cell assembly (CR2032) was carried out with symmetrical active carbons (ASAC-30, Canada) electrodes and a spetrator (GF/F), GCD cylcing ability was further tested in a NEWARE battery cycler (CT-4008T-5V50mA-164, Shenzhen, China).

The gravimetric capacitance (C) based on GCD curves was calculated according to equation [2]:

$$C = (I \cdot \Delta t_1)/(2m \cdot \Delta V) \quad [2]$$

where Δt_1 (s) is the discharge time, ΔV (V) is operation voltage excluding the IR drop, I and m are applied current and active material loading on one electrode, respectively.

The Coulombic efficiency (CE) was determined according to equation [3]:

$$CE = \Delta t_1/\Delta t_2 \quad [3]$$

where Δt_2 (s) is the charge time.

Computational details

All molecular dynamic (MD) simulations were carried out using the Forcite package of Material Studio software. The forcefield was simulated with COMPASS. $ALE_{6.6}$ and $ALE\text{-}DME_{6.6}$ with molar ratios as shown in Table S1 were added to a 35×35×35 $Å^3$ box, respectively. The systems were equilibrated at 298 K in the NVT ensemble for 50 ps with a timestep of 1.0 fs, and the Nose thermostat was used to control the temperature.[2]

Density functional theory (DFT) computations were carried out using the $Dmol^3$ code[3,4] within the generalized gradient approximation (GGA) method in the form of the Perdew-Burke-Ernzerhof (PBE)[4,5]. The convergence energy and Monkhorst-Pack k-point mesh was set to 1.0×10^{-5} Ha and 3×3×1, respectively. During geometry optimization, the convergence tolerance was set as 1.0×10^{-5} eV for energy, and 0.004 Ha $Å^{-1}$ for force. A vacuum of 20 Å was used to avoid interactions between periodic images.

Results and Discussion

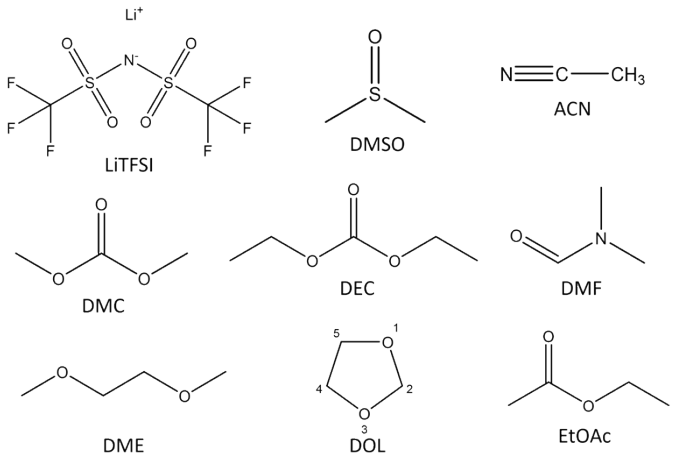

Figure S1. Molecular structures of LiTFSI and different solvents.

Table S1. Molar ratios of LiTFSI, DMSO, H_2O and different solvents in various electrolytes.

Sample	Molar ratio			
	LiTFSI	**DMSO**	**H_2O**	**Solvent**
$ALE_{6.6}$	0.753	1	2	--
$ALE\text{-}ACN_{6.6}$	0.753	0.75	1.5	0.695
$ALE\text{-}DMC_{6.6}$	0.753	0.75	1.5	0.317
$ALE\text{-}DEC_{6.6}$	0.753	0.75	1.5	0.242
$ALE\text{-}DMF_{6.6}$	0.753	0.75	1.5	0.391
$ALE\text{-}DME_{6.6}$	0.753	0.75	1.5	0.317
$ALE\text{-}DOL_{6.6}$	0.753	0.75	1.5	0.386
$ALE\text{-}EtOAc_{6.6}$	0.753	0.75	1.5	0.324

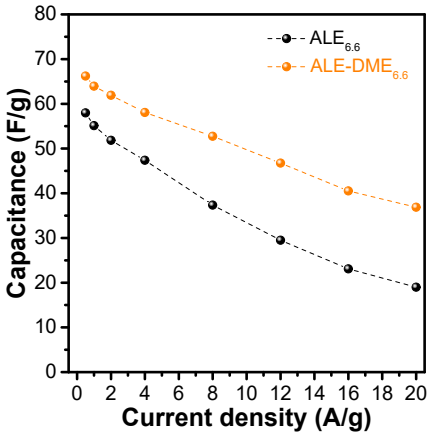

Figure S2. Capacitance of various ALE-based electrolytes at different current densities.

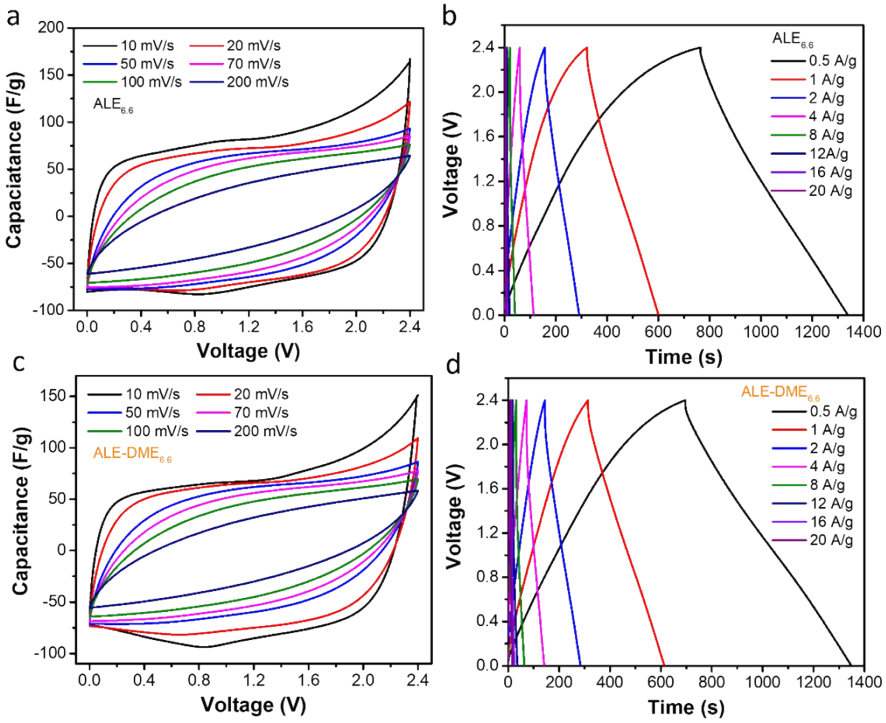

Figure S3. CV curves at different scan rates and GCD profiles at different current densities of $ALE_{6.6}$ and $ALE\text{-}DME_{6.6}$ electrolytes measured at room temperature.

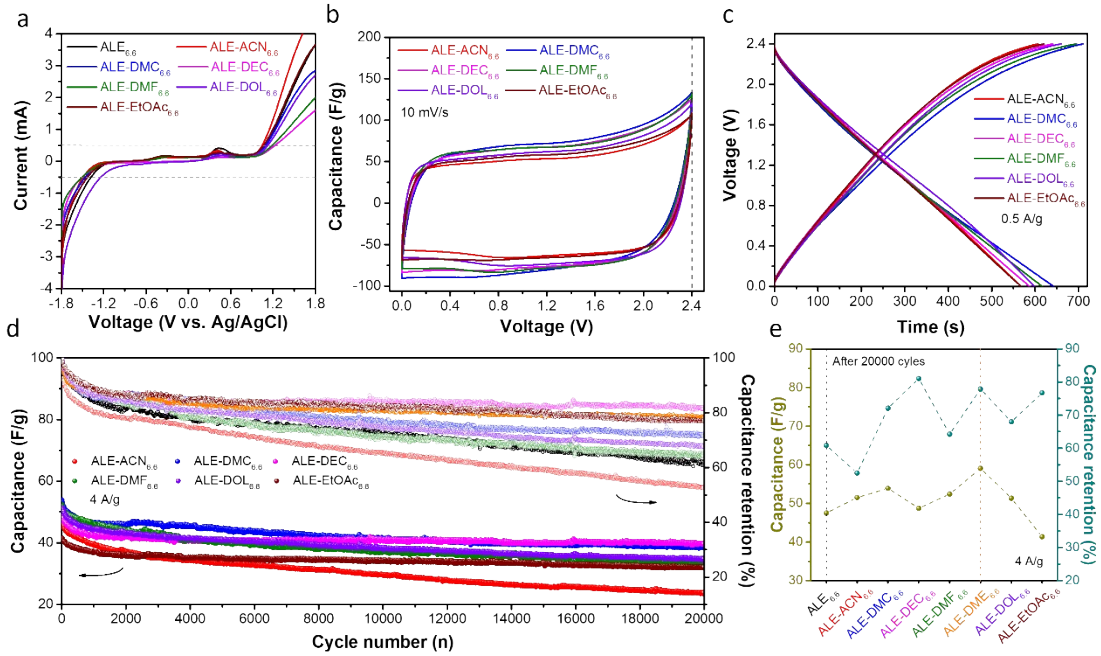

Figure S4. Electrochemical performance of various ALE-based electrolytes at room temperature. a) ESWs measured with linear sweep voltammetry at a scan rate of 10 mV s^{-1}. b) CV curve at a scan rate of 10 mV s^{-1}. (c) GCD profiles at a current density of 0.5 A g^{-1}. (d) Cycling performance at a current density of 4 A g^{-1}. e) Capacitance before cycling and capacitance retention after 2000 cycles at 4 A g^{-1}.

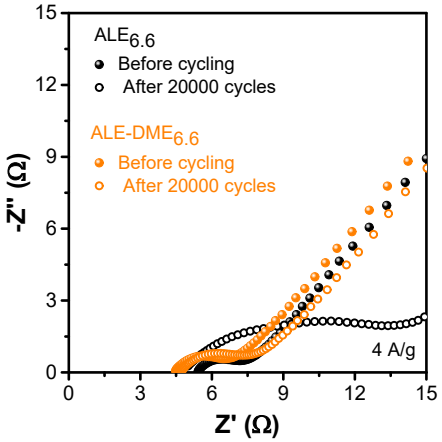

Figure S5. Nyquist plots of $ALE_{6.6}$ and $ALE\text{-}DME_{6.6}$ electrolytes measured before cycling and after 20000 cycles at room temperature with high frequency region magnification.

Table S2. Specific values of R_e and R_{ct} before and after 20000 cycling.

Sample	Before cycling		After 20000 cycles	
	R_e	R_{ct}	R_e	R_{ct}
$ALE_{6.6}$	5.06	2.37	5.42	8.63
$ALE\text{-}ACN_{6.6}$	2.92	1.59	10.36	28.25
$ALE\text{-}DMC_{6.6}$	4.85	2.00	7.36	2.49
$ALE\text{-}DEC_{6.6}$	5.68	2.29	6.85	3.46
$ALE\text{-}DMF_{6.6}$	5.51	2.16	23.60	4.90
$ALE\text{-}DME_{6.6}$	4.47	1.96	4.78	2.65
$ALE\text{-}DOL_{6.6}$	4.52	2.03	6.95	5.02
$ALE\text{-}EtOAc_{6.6}$	5.17	1.92	13.52	5.54

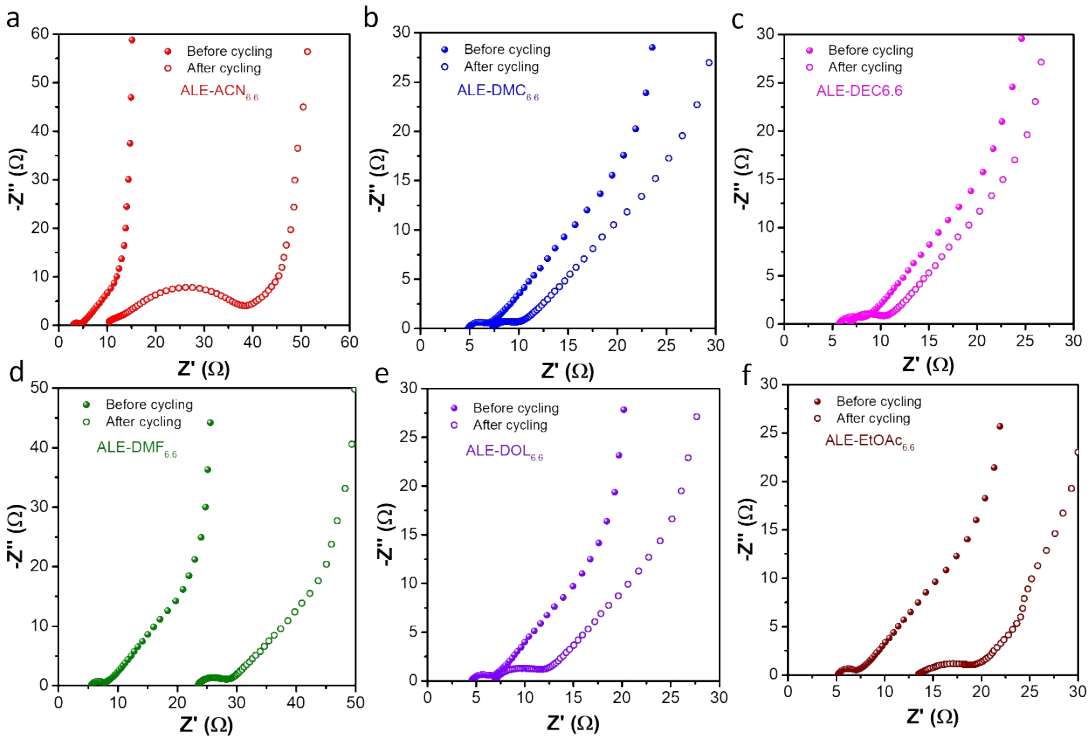

Figure S6. Nyquist plots of other ALE-based electrolytes measured before cycling and after 20000 cycles at room temperature.

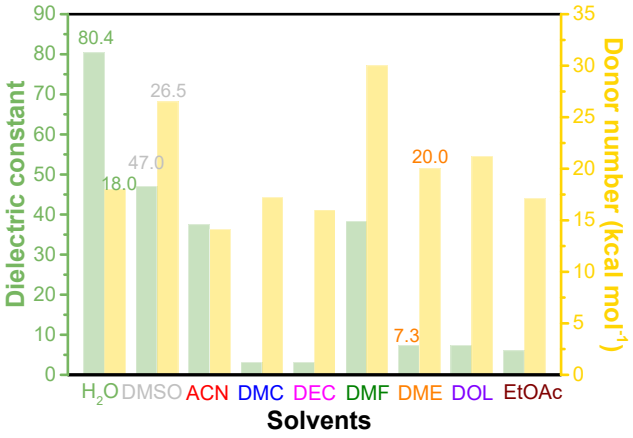

Figure S7. Dielectric constant and DNs of H_2O and different organic solvents.

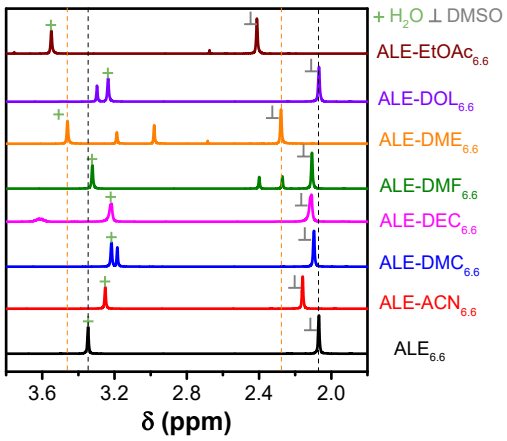

Figure S8. ^{1}H NMR spectra of $ALE_{6.6}$ and ALE-based electrolytes.

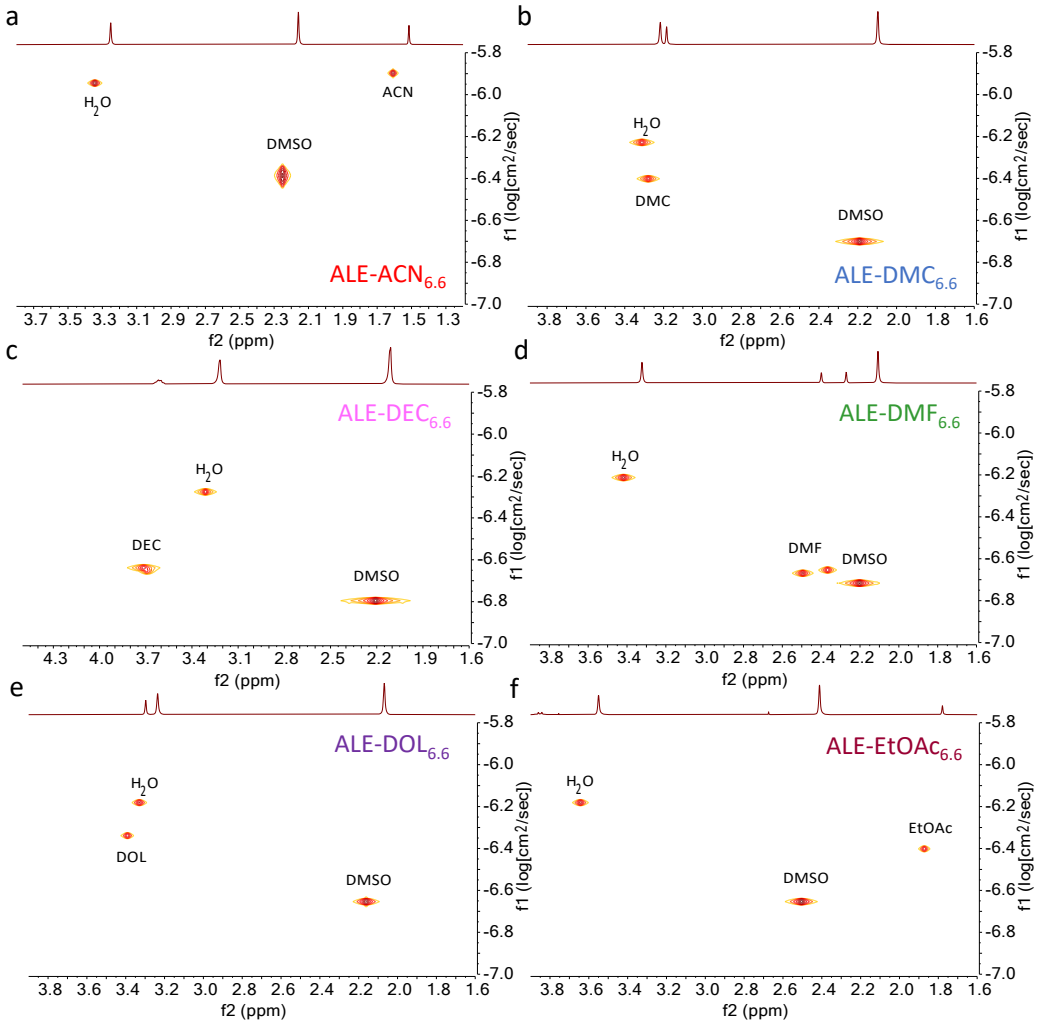

Figure S9. ^{1}H DOSY spectra of the rest ALE-based electrolytes.

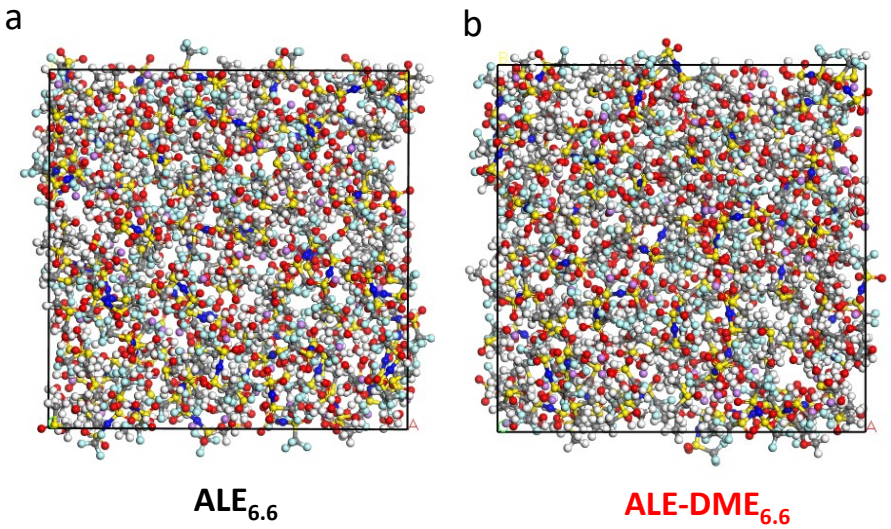

Figure S10. Snapshots of a) $ALE_{6.6}$ and b) $ALE\text{-}DME_{6.6}$ electrolyte structures in MD simulation.

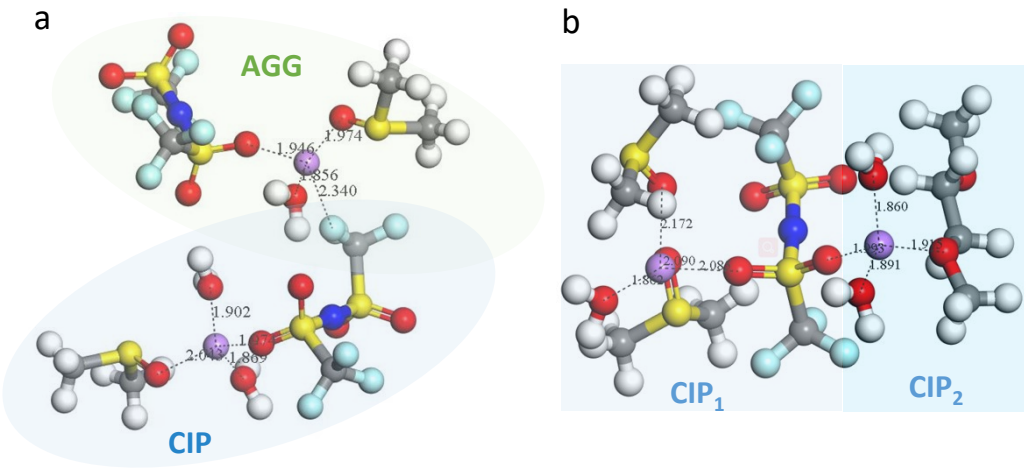

Figure S11. Structures of the most probably inner solvation shells of a) $ALE_{6.6}$ and b) $ALE\text{-}DME_{6.6}$ electrolytes from MD simulation.

In ALE-based electrolytes, the solvent molecules are outnumbered by Li^+ and/or $TFSI^-$ susceptible to solvation so that ionic species such as contact ion pairs (CIPs) and ionic aggregates (AGGs) co-exist in the highly concentrated solution. In Figure S11a, typical CIP and AGG species are sharing the one or two anions of $TFSI^-$ in $ALE_{6.6}$ electrolyte considering the participation of DMSO and H_2O. As elucidated in previous work, we hypnotized the formula of Li^+-solvated DMSO/H_2O complexes and $TFSI^-$ anions as $Li^+(DMSO)_a(H_2O)_b(TFSI^-)_c$ with a + b + c= 4 according to CIP and AGG formation.[1] The corresponding results delivered the proof of solvation affinity and structure stability among LiTFSI and eutectic mixtures of DMSO/H_2O. Furthermore, the DME regulator introduced a CIP difference as CP_1 (*e.g.*, Li^+-solvated with two DMSO, one H_2O, and $TFSI^-$) and CP_2 (*e.g.*, Li^+-solvated with one DME, two H_2O, and $TFSI^-$) (Figure S11b). This regulation agent (DME) shows the ability to weaken the solvation ability of the two oxygen atoms or ethoxy groups, promoting an increased number of $TFSI^-$ solvating structures (*e.g.,* CIPs). These results above are evidential to combine Raman, FTIR, MD, and electrochemical experimental consequence, which generally provides support from molecular views.

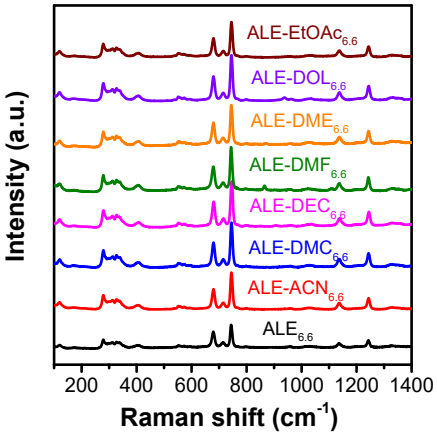

Figure S12. Raman spectrum of $ALE_{6.6}$ and ALE-based electrolytes in the range of 100–1400 cm^{-1}.

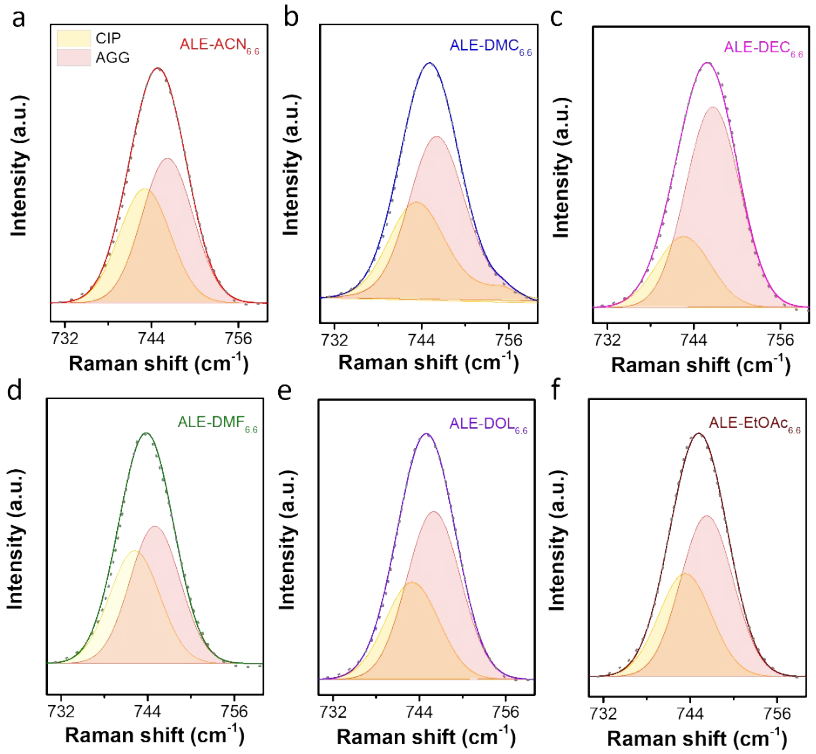

Figure S13. Integrated Raman spectrum of the rest ALE-based electrolytes in the range of 730–760 cm^{-1}.

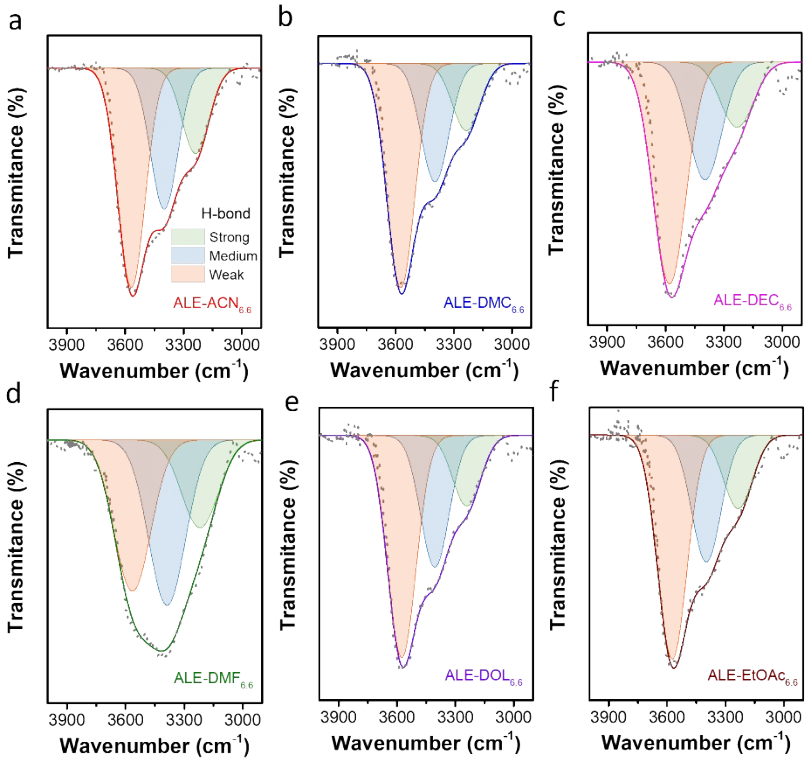

Figure S14. Integrated FTIR spectrum of the rest ALE-based electrolytes in the range of 2900–4000 cm^{-1}.

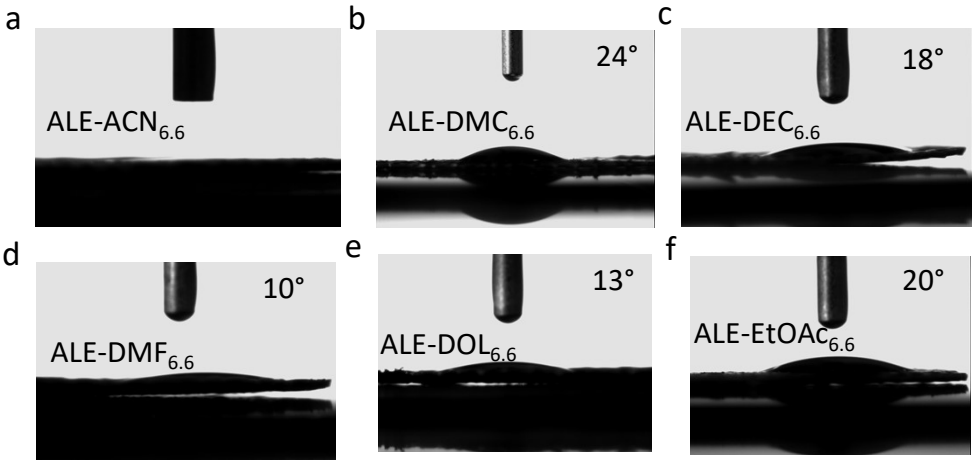

Figure S15. Contact angle measurements of the rest ALE-based electrolytes.

Figure S16. Flammability tests of $ALE_{6.6}$ and ALE-based electrolytes.

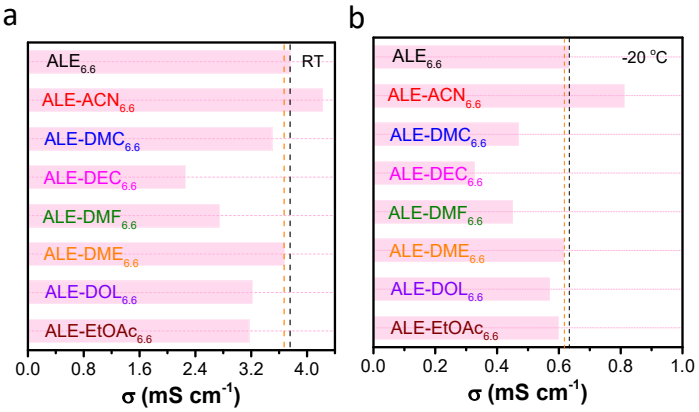

Figure S17. Ionic conductivity of $ALE_{6.6}$ and ALE-based electrolytes at a) room temperature (RT) and b) –20 °C.

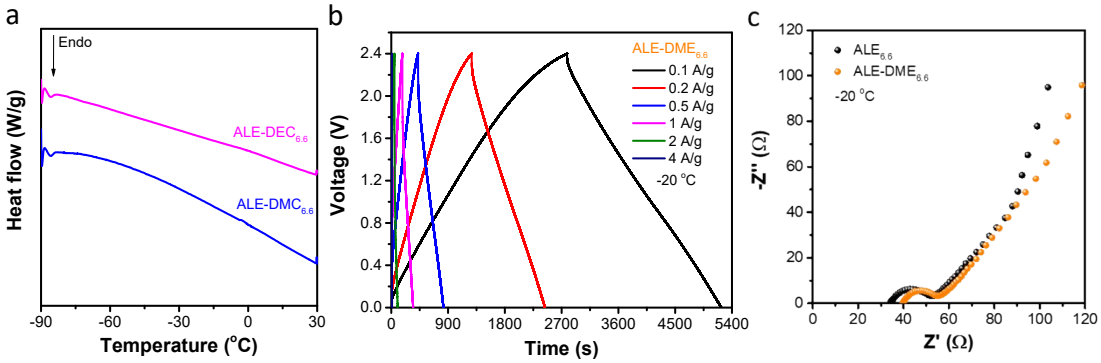

Figure S18. A) DSC spectra of $ALE\text{-}DMC_{6.6}$ and $ALE\text{-}DEC_{6.6}$. b) GCD profiles of $ALE\text{-}DME_{6.6}$ with different current densities at –20 °C. c) Nyquist plots of $ALE_{6.6}$ and $ALE\text{-}DME_{6.6}$ at –20 °C.

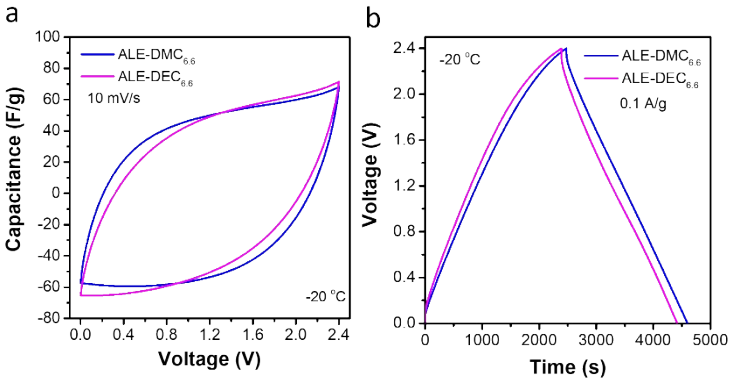

Figure S19. a) CV curves at 10 mV s^{-1} b) GCD profiles at 0.1 A g^{-1} of ALE-$DMC_{6.6}$ and ALE-$DEC_{6.6}$ at –20 °C.

Table S3. The comparison of capacitance, cyclability, and capacity retention after cycling reported for SCs using different electrodes and electrolytes and operating at different temperatures.

Electrolytes	**Electrodes**	**T (°C)**	**Capacitance (F g^{-1})**	**Cycles number (n)**	**Capacitance Retention**	**Ref.**
ALE-$DME_{6.6}$	ASAC-30	25	66.2 (0.5 A g^{-1})	20000 (4 A g^{-1})	~80.0%	This work
		–20	51.6 (0.1 A g^{-1})	8000 (1 A g^{-1})	80.0%	
$ALE_{6.6}$	ASAC-30	25	58.0 (0.5 A g^{-1})	20000 (4 A g^{-1})	60.0%	This work
20m LiTFSI-H_2O	Petal-derived porous carbon	25	50.0 (0.5 A g^{-1})	5000 (2 A g^{-1})	84.0%	[7]
		–10	34.0 (0.5 A g^{-1})	5000 (2 A g^{-1})	38.0%	
5m LiTFSI-H_2O/CH_3CN	Activated carbon	25	27.0 (1 A g^{-1})	14000 (6 A g^{-1})	81.0%	[8]
		–30	21.8 (1 A g^{-1})	--	--	
$(NaClO_4)_{1.7}$-$(H_2O)_{4.7}$/$(CH_3CN)_3$	Activated carbon	20	31.8 (20 mV s^{-1})	--	--	[9]
		–50	27.5 (20 mV s^{-1})	ca. 7000 (2 A g^{-1})	91.0%	
3.5m $Mg(ClO_4)_2$ hydrated eutectic	Activated carbon	25	24.6 (1 A g^{-1})	10000 (4 A g^{-1})	92.6%	[10]
		–40	18.6 (1 A g^{-1})	6000 (4 A g^{-1})	ca. 100%	
3m LiTFSI sulfolane/H_2O	Activated carbon	25	106.0 (0.5 1 A g^{-1})	10000 (10 A g^{-1})	93.0%	[11]

References

[1] X. Lu, R.-J. Jiménez-Riobóo, D. Leech, M.-C. Gutiérrez, M.-L. Ferrer, Francisco del Monte. Aqueous-Eutectic-in-Salt Electrolytes for High-Energy-Density Supercapacitors with an Operational Temperature Window of 100 °C, from −35 to +65 °C. *ACS Appl. Mater. Interfaces* **2020**, 12, 26, 29181–29193.

[2] H. J. Liang, Z.Y. Gu, X. X. Zhao, J.Z. Guo, J. L. Yang, W.H. Li, B. Li, Z. M. Liu, W.L. Li, X. L. Wu. Ether-based electrolyte chemistry towards high-voltage and long-life Na-ion full batteries. *Angew. Chem. Int. Ed.* **2021**, 60, 2–12.

[3] B. G. Johnson, P. M. W. Gill, J. A. People. The performance of a family of density functional methods. *J. Chem. Phys.* **1993**, 98, 5612-5626.

[4] J.P. Perdew, J.A. Chevary, S.H. Vosko, K.A. Jackson, M.R. Pederson, D.J. Singh, C. Fiolhais. Atoms, molecules, solids, and surfaces: applications of the generalized gradient approximation for exchange and correlation. *Phys. Rev. B* **1992**,46, 6671.

[5] J.P. Perdew, K. Burker, Y. Wang. Generalized gradient approximation for the exchange-correlation hole of a many-electron system. *Phys. Rev. B* **1996**, 54, 16533–16539.

[6] J.P. Perdew, Y. Wang. Accurate and simple analytic representation of the electron gas correlation energy. *Phys. Rev. B* **1992**, 45, 13244.

[7] C. Naresh, N.C. Osti, A. Gallegos, B. Dyatkin, J. Wu, Y. Gogotsi, E. Mamontov Mixed ionic liquid improves electrolyte dynamics in supercapacitors. *J. Phys. Chem. C* **2018**, 122, 10476-10481.

[8] Q. Dou, S. Lei, D.-.W. Wang, Q. Zhang, D. Xiao, H. Guo, A. Wang, H. Yang, Y. Li, S. Shi, X. Yan. Safe and high-rate supercapacitors based on an ‘‘Acetonitrile/Water in Salt’’ hybrid electrolyte. *Energy Environ. Sci.* **2018**, 11, 3212-3219.

[9] Y. Sun, Y. Wang, L. Liu, B. Liu, Q. Zhang, D. Wu, H. Zhang, X. Yan. Towards the understanding of acetonitrile suppressing salt precipitation mechanism in a water-in-salt electrolyte for low-temperature supercapacitors. *J. Mater. Chem. A* **2020**, 8, 17998-11685.

[10] M. Zhong, Q.F. Tang, Y.W. Zhu, X.Y. Chen, Z.J. Zhang. An alternative electrolyte of deep eutectic solvent by choline chloride and ethylene glycol for wide temperature range supercapacitors. *J. Power Sources* **2020**, 452, 227847.

[11] X., Cheng, J., Yuan, J., Hu, S., Chen, H., Yan, W., Yang, W., Li, Y., Dai. 2.5 V high-performance aqueous and semi-solid-state symmetric supercapacitors enabled by 3 m sulfolane-saturated aqueous electrolytes. *Energy Technol.* **2022**, 2200157.